Heliyon 8 (2022) e12346

Contents lists available at ScienceDirect

Heliyon

journal homepage: www.cell.com/heliyon

Research article

A hybrid photonic-plasmonic resonator based on a partially encapsulated 1D photonic crystal waveguide and a plasmonic nanoparticle

Belkıs Gökbulut *

Institute for Data Science and Artificial Intelligence, Bogazici University, Bebek, 34342 Istanbul, Turkey

ARTICLE INFO

Keywords:
Photonic crystal
Hybrid resonator
Optical mode
Plasmonic nanoparticle
Spontaneous emission

ABSTRACT

In this paper, a hybrid photonic-plasmonic resonator is proposed. The device consists of a partially encapsulated 1D photonic crystal waveguide and a plasmonic nanoparticle to yield high radiation efficiency for integrated photonic platforms, owing to a high *Q*-factor and a small mode volume. The design of the resonator is accomplished in two consecutive steps: first of all, a partially encapsulated photonic crystal nanobeam with a robust mechanical stability and a high-*Q* factor is prepared; secondly, a plasmonic nanoparticle is placed on the surface of the nanobeam to interact the optical mode with the localized surface plasmons of the gold nanoparticle which is being present in the vicinity of the radiating dipole. Strongly enhanced electromagnetic field, regenerated through the optical mode field inside the hybrid resonator, enables to reduce the optical mode volume of the device and significantly enhance the Purcell factor.

1. Introduction

In the last decade, photonic crystals have attracted a significant research interest in integrated photonic platforms [1], quantum information technologies [2], electro-optical systems [3] along with various research fields like cavity quantum electrodynamics [4], random light localization [5], applications of the optical trapping for particles with diameters on the order of nanometers [6], wavelength-division demultiplexing [7], and the second harmonic generation of light [8]. Because of the capabilities of these resonators; having a high-quality factor (*Q*-factor) for temporal confinement of the optical power and a small mode volume for strong spatial confinement of the photons, one may improve the performance of the photonic devices [9]. Their outcome is conventionally measured through the strong enhancement of the spontaneous emission rate, which is elegantly pronounced by the Purcell factor.

Photonic crystals are usually designed using free-standing geometries to maximize the refractive index contrast between the waveguide and the surrounding medium of the resonator to achieve high *Q*-factors [10]. However, these devices have been demonstrated to be almost incompatible with comprehensive semiconductor industry processes, which are crucial for development of the integrated photonic technologies [11]. The main difficulty is that the floating membranes are susceptible to microfabrication techniques like resist spinning for lithographic processes. The other challenge is that the dry transfer techniques to construct van der Waals heterostructures would also result in a damage to the floating membrane [12]. It would also be stringent to integrate several 2D materials on the same photonic chip, which is not mechanically stable and robust because of the fluctuant membrane. As an alternative, these devices would be encapsulated with polymer layers to avoid free-standing structures and susceptibility for further manufacturing processes [13, 14]. In addition to all these, the encapsulation also facilitates the characterization of the devices as the mechanical robustness allows to easily remove 2D materials from the surface of the membrane to renewably integrate the same materials with the desired properties on the same photonic structure. However, encapsulated photonic crystals have reduced refractive index contrasts between the waveguide and the surrounding medium, compared to their air-bridged counterparts, which leads to a substantially decreased *Q*-factor [12].

In this paper, a photonic device is initially designed as a partially encapsulated structure in which the substrate and top cover material are chosen to be SiO_2 and PMMA, respectively, and both sides of the nanobeam are chosen to be air cladding, which is almost symmetric in every axis, yielding a high *Q*-factor and mechanical robustness to propose as an alternative to air-bridged photonic crystals for high radiation efficiency.

The other crucial factor that affects the radiation efficiency of the photonic devices is the mode volume. In recent years, 1D photonic crystal cavities, owing to a smaller mode volume and more compact structural designs compared to 2D photonic crystal cavities, have been

* Corresponding author.
E-mail address: belkis.gokbulut@boun.edu.tr.

https://doi.org/10.1016/j.heliyon.2022.e12346
Received 24 November 2022; Received in revised form 6 December 2022; Accepted 7 December 2022

demonstrated to be the superior resonator choice for photonic research and device technologies [15, 16, 17] in the area of quantum optics [18], non-linear optics [19], optomechanics [20], light modulators [21], and laser applications [22]. Especially, when 1D photonic crystals are designed to have a high *Q*-factor and an ultra-small mode volume, they can even be used in the detection of extremely sensitive chemical and biological applications [23, 24]. In general, although photonic crystal cavities are designed in accordance with a high *Q*-factor, depending on the materials and design parameters, nevertheless, limited reduction in the size of such photonic structures prevents obtaining very small optical mode volumes upon their fabrication processes [25]. On the other hand, it is possible to produce a photonic device with a high *Q*-factor and a small mode volume using a hybrid device consisting of a photonic cavity and plasmonic nanoparticles [26, 27]. Although hybrid dielectric microcavities coated by plasmonic layers have been reported to have low-*Q* factors [28], integration of plasmonic nanoparticles into photonic crystal cavities have been demonstrated that the *Q*-factor of the photonic device in concern is relatively retained with improved device characteristics [29]. As a result of the interaction between the photonic cavity mode and the surface plasmons of the metal nanoparticles, light waves concentrate within a very small volume, reducing the optical mode volume enormously [30]. Localized light waves in a small volume enhance light−matter interactions; thus, enabling highly efficient laser radiation with improved spontaneous emission. Moreover, in the regime of cavity quantum electrodynamics, it is possible to reduce the laser dimensions to utilize them in quantum information technologies. For example, in order to produce an efficient low-threshold nanolaser, semiconductor nanocrystals are usually preferred as active media for obtaining radiation [31]. However, plasmonic nanostructures in the vicinity of quantum sources result in a loss in the intensity of the emitters. Additionally, the excessive energy and electron transfer mechanisms between the metal particles and the dipoles of the quantum sources dominate the enhancement of the spontaneous emission [32].

In this work, a modelling of a hybrid device is proposed to develop an efficient photonic device with a high *Q*-factor and small mode volume, which consists of a partially encapsulated 1D photonic crystal waveguide and a single gold nanosphere. After a partially encapsulated photonic crystal cavity is designed, a gold nanoparticle is placed on the surface of the PMMA surface to regenerate a hybrid photonic-plasmonic resonator. The mode volume of the structure significantly decreases through the coupling of the cavity mode to the localized surface plasmons of a single gold nanoparticle to strongly confine the electromagnetic field in the photonic device. The polymer layer between the dipole on the surface of the photonic crystal cavity and the surface plasmons of the metal nanoparticle provides a controllable distance between the gold nanoparticle and the light emitter for efficient dipole-surface plasmon interaction as it almost eliminates the quenching mechanism. Our numerical analyses demonstrate that the enhancement of the Purcell factor of 1.3×10^4 is achieved, which is considerably higher than the previously reported values for encapsulated photonic crystals. Thus, a compact and elegant photonic design, which is simple to produce, is presented to yield high radiation efficiency. The hybrid resonator proposed in this paper is envisaged to be highly promising for remarkable advances in integrated photonic platforms, quantum information technologies, and laser applications.

2. The design of the photonic device

In this work, Finite Difference Time Domain Technique (FDTD) is utilized to design a 1D SiN photonic crystal with a high *Q*-factor and a small mode volume, operating in the visible wavelength region. MEEP software is utilized to determine the bandgap of the structure. A defect mode is introduced to obtain a radiation frequency at the desired wavelength of 561.5 nm. 1D photonic crystal geometry is preferred since 1D crystals have larger band gaps when compared to that of the 2D photonic crystals [33]. A SiN layer, with a refractive index of 2.05 and a thickness of 218.33 nm, is used as the nanobeam material since SiN has an ultralow absorption coefficient in the near-visible wavelength range [34]. Additionally, the photonic device is designed as a partially encapsulated structure of which the substrate material is chosen to be SiO_2 and the top cover material is preferred to be PMMA. The perspective view of the partially encapsulated photonic crystal resonator along with its dimensions is illustrated in Figure 1a. The SiN thickness and the nanobeam width are given by $b = 218.33$ nm and $a = 400$ nm, and the thickness of the PMMA layer on the surface of the SiN nanobeam is determined to be $c = 40$ nm Figure 1b shows the cross-sectional view of the device with related indices of refraction.

The main reason for choosing the PMMA as the top cover is because it has an index of refraction 1.495, which is close to the refractive index of SiO_2 substrate 1.46. This index matching is crucial since the index of refraction around the photonic crystal significantly affects the quality factor of the device [35]. Another reason to use the PMMA as the top cover of the structure is that it can be removed easily without damaging the photonic crystal [36] when additional processes are needed. Thus, depending on the application, the PMMA can be ripped off and coated again at the desired thickness and geometry [14]. The encapsulation also provides a mechanical stability and robustness; nonetheless, it reduces the *Q*-factor of the device because of the decreased refractive index contrasts between the waveguide and the surrounding medium. To overcome this problem, in our photonic design, both sides of the nanobeam in the x-axis direction is chosen to be air cladding, which is shown in Figure 1a. Thus, as the index matching is partially ensured by SiO_2 substrate-PMMA layer in the z-axis and air claddings on each side in the

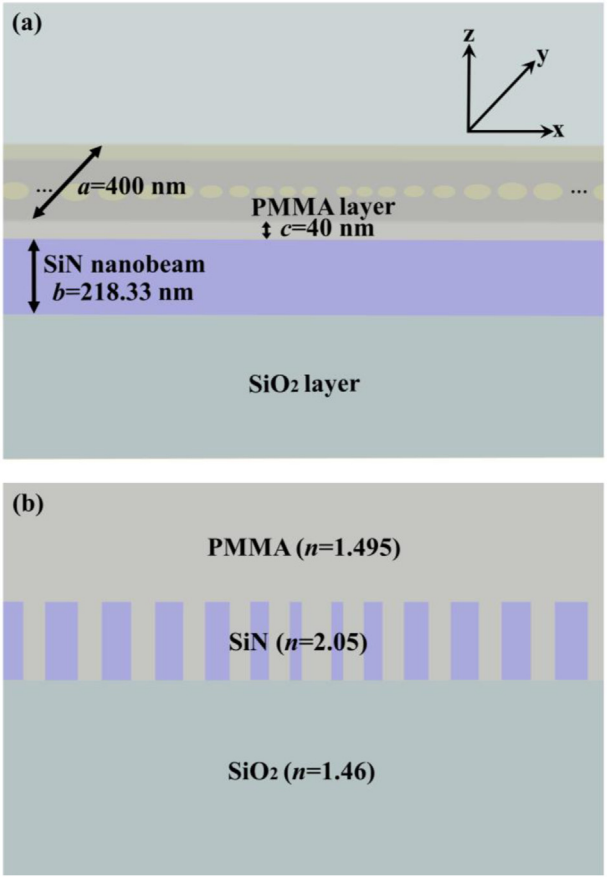

Figure 1. (a) Perspective view of the partially encapsulated photonic crystal waveguide along with its dimensions. (b) The cross-sectional view of the designed photonic structure with related indices of refraction of the materials that form the structure.

x-axis, the *Q*-factor of the photonic device is significantly improved compared to the completely encapsulated photonic crystal waveguides.

Simulation parameters are optimized to enhance the *Q*-factor of the resonant mode. A sketch of the photonic nanobeam with its optimized design parameters is given in Figure 2. On each side of the 1D photonic crystal, there are forty mirror holes as Bragg reflectors, which have fixed diameter and lattice constant labeled as *D* and *p*, respectively, and seven taper holes that have linearly decreasing radius and lattice constant towards the center of the photonic crystal. Cavity length (L_c) is the distance between the innermost holes, which is equal to 159 nm in our design. The nanobeam width is also shown in Figure 2, with a symbol of *a*. In the simulations, for a photonic crystal waveguide with a width of 400 nm, the optimized parameters of the mirror hole diameter and the lattice constant are determined to be 120 nm and 170 nm, respectively. The taper part has been optimized in order to minimize the modal mismatch between the waveguide mode and the photonic crystal Bloch mode [37]. Thus, the smallest diameter of the mirror hole at the taper part is determined to be 110 nm. The PMMA layer is also placed on the surface of the nanobeam and the plasmonic nanoparticle is placed on the surface of the PMMA layer to facilitate an efficient dipole-surface plasmon interaction.

3. Results and discussion

The transverse electric field (TE) polarized bandgap simulation results of the outermost mirror hole and the innermost mirror hole are given in Figure 3.

In this graph, red and dark blue colored lines represent the bandgap of the innermost and outermost mirror holes, respectively. The defect band, light cone and the light line of SiO_2 below the SiN layer, are also shown in Figure 3. According to these results, the defect band is determined to be at the wavelength of 561.5 nm.

Figure 4 shows the cross-sectional view of the simulated electric field intensity distribution of a unit cell in the defect band in each dimension. Figure 4a shows the top view of the electric field distribution for the unit cell in the xy plane. In Figure 4a, the boundaries of the photonic crystal waveguide along the x-axis are given by white lines and the perimeter of the nanohole with a diameter of $D = 110$ nm is also shown with a white circle on the xy plane. The width of the waveguide is demonstrated by a scale bar ($a = 400$ nm). Figure 4b and 4c show the side views of the electric field distributions in the xz and yz planes, respectively. In Figure 4b, the boundaries of the nanohole in xz direction are shown by the white lines and the dimensions of the hole depth and diameter are given by scale bars. In Figure 4c, the boundaries of the two nanoholes are emphasized by white lines in yz direction. The hole depth is given by the scale bar ($b = 218.33$ nm). The electric field intensity for the unit cell is scaled by a color bar, as shown in Figure 4.

The Bloch mode formula of the mirror holes over a unit cell is given in Eq. (1) in which x is the direction of the repeating mirror holes and **u** represents the function of the periodicity [37].

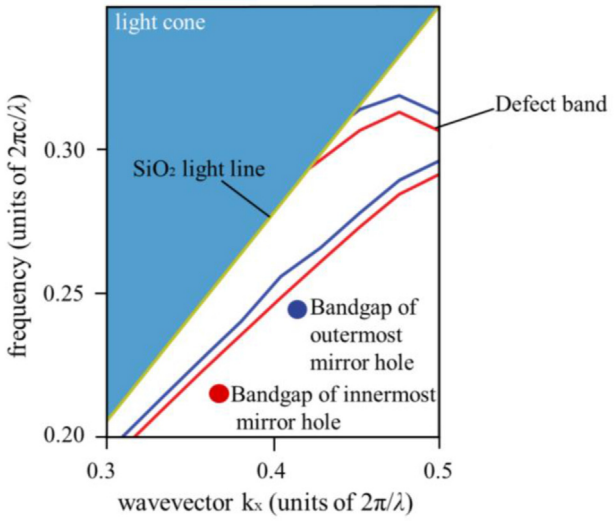

Figure 3. Bandgap simulation results of the mirror holes and the innermost mirror hole.

$$\mathbf{H}_{n,k_z,\mathbf{k}}(\mathbf{r}) = e^{i\mathbf{k}\cdot\rho} e^{ik_x x} \mathbf{u}_{n,k_x,\mathbf{k}}(x), \tag{1}$$

FDTD method is also used to obtain the photoluminescence spectra of the dipole coupled into the resonant mode of the device. After using the optimization toolbox of the FDTD solver module of the program Lumerical Ltd., the *Q*-factor of the device is calculated to be $2.05 \times 10^5 \pm 1.47$, which is at least two times higher than the previously reported values in the literature [35, 38]. Calculated spectra of the device are given in Figure 5a and 5b for both cases when a broadband source and a dipole source are used, respectively. When the broadband source is used, a fundamental waveguide mode appears at the wavelength of 561.5 nm, in addition to the higher order waveguide modes, which appear between the wavelengths of 200 nm and 300 nm, as shown in Figure 5a. These higher order modes are basically generated by the confinement of the photons within the slab waveguide, forming subbands in the structure [39]. However, it has been demonstrated that when a higher order mode is located near the peak wavelength of the fundamental mode, the intensities of both the fundamental and the higher order mode rise upon the increase of the pump power, reducing the efficiency of the fundamental mode [40]. On the other hand, when the wavelengths of the higher order modes are distant from that of the fundamental waveguide mode, as seen in Figure 5a, the fundamental mode dominates the higher order modes. Figure 5b shows the PL spectrum of the fundamental waveguide mode when the central wavelength of the dipole source is set to the wavelength of 561.5 nm with a bandwidth of 46 nm.

Refractive index and electric field distribution profiles at the central cross section of the photonic resonator are shown in Figure 6a and 6b,

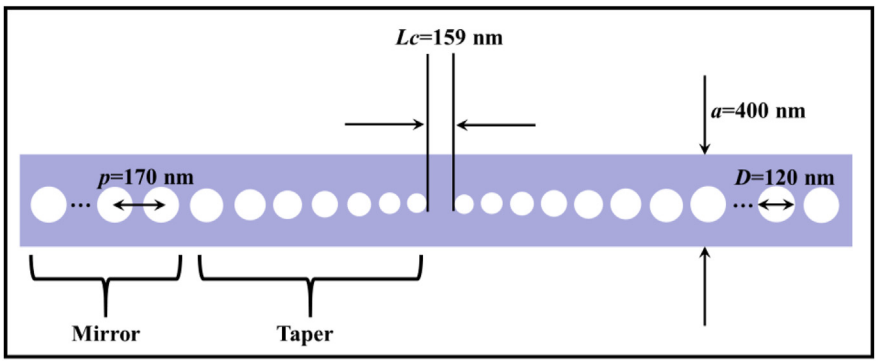

Figure 2. Sketch of the nanobeam including the optimized simulation parameters.

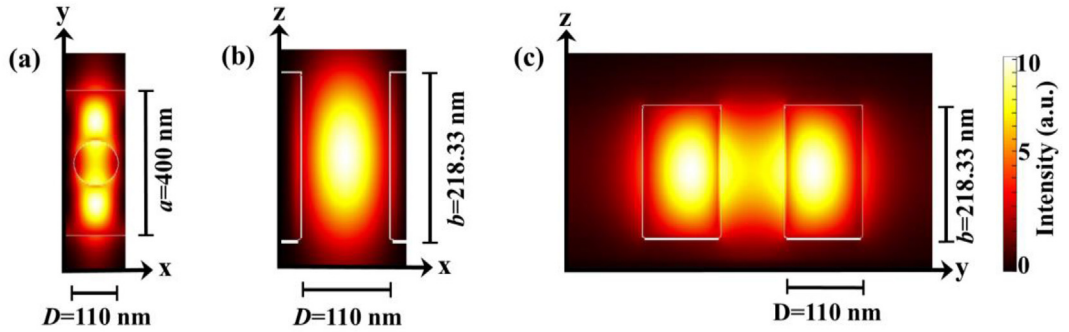

Figure 4. The simulated electric field intensity distribution of a unit cell in defect band. The profiles are obtained in xy, xz and yz planes.

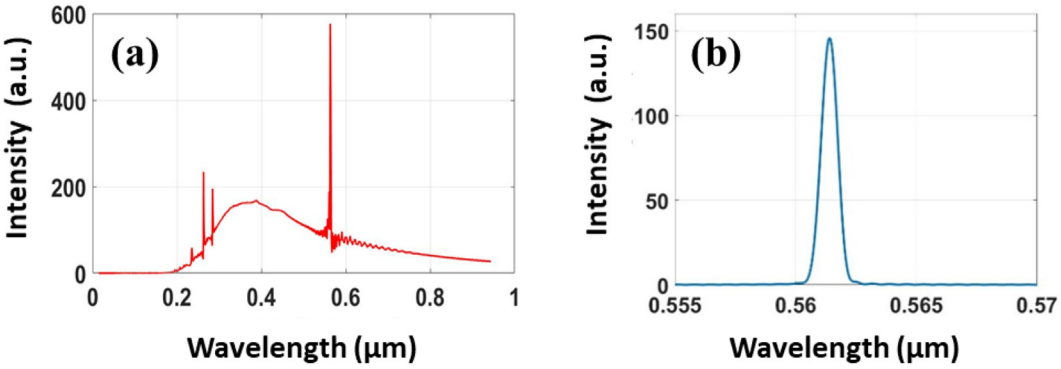

Figure 5. Calculated spectra of the device using a) a broadband and b) a dipole source.

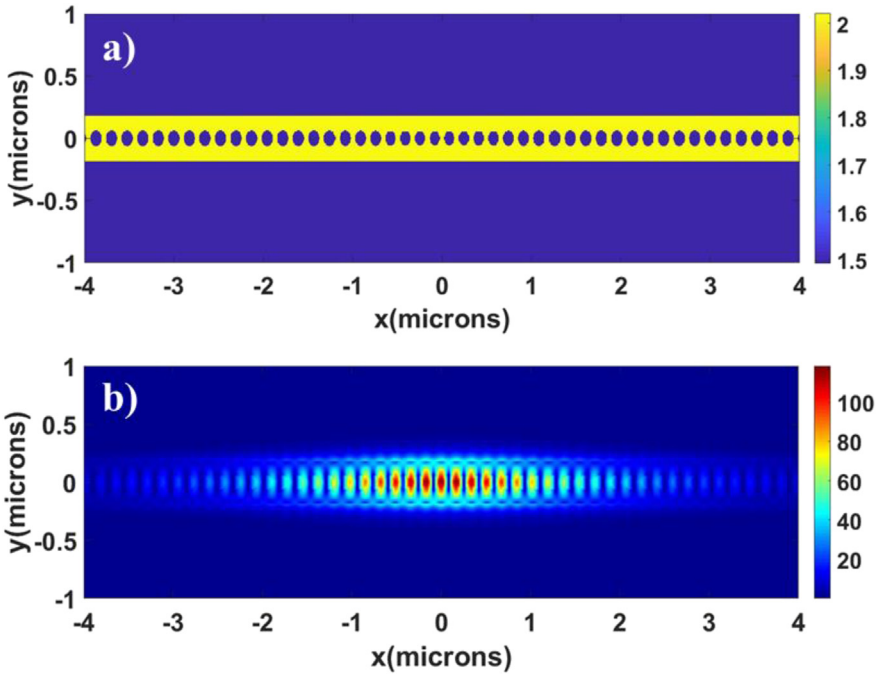

Figure 6. a) Refractive index and b) the electric field distribution profile at the central cross section of the photonic resonator. One should notice that in Figure 6a; on each side of the 1D photonic crystal, there are forty mirror holes as Bragg reflectors, which have fixed diameter and lattice constant and seven taper holes that have linearly decreasing radius and lattice constant towards the centre of the photonic crystal.

respectively. For visual purposes, the region which involves only the thirty-two of the mirror holes out of eighty is illustrated. The mode volume of the designed photonic crystal cavity is calculated to be around 9.8 $(\lambda/n)^3$.

Decreasing the mode volume of the photonic device is crucial to design highly efficient and low-threshold lasers as the photonic resonators with a high-quality factor and a small mode volume reduce the amount of active material in the cavity and enhances the spontaneous

emission rate of the fluorescent emitters like quantum dots or dye molecules [41]. For the second construction stage of the photonic device, a plasmonic nanoparticle with a diameter of 19 nm, is finally placed at the center of the PMMA layer surface to regenerate a hybrid photonic-plasmonic resonator. The mode volume of the nanobeam decreases through the coupling of the cavity mode to the localized surface plasmons of a single gold nanoparticle to strongly confine the electromagnetic field in the photonic device [42]. Nevertheless, metal particles located at the vicinity of the fluorescent emitters result in a significant loss in the intensity of these quantum light sources through a process called quenching [43]. Accordingly, in our photonic system, after a dipole, which is assumed to be a fluorescent quantum dot, is placed on the surface of the structure, the photonic crystal nanobeam is partially coated by a PMMA layer. In a photonic design with a certain thickness of the PMMA layer on the surface of the nanobeam to originate a controllable distance between the gold nanoparticle and the dipole of the quantum source, as the mode volume of the structure is reduced, almost no considerably change is observed in the quality factor; and hence, the quenching mechanism is primarily prevented.

Strong confinement of the cavity mode field of the photonic crystal waveguide at nanoscale is essentially based on the absorption characteristics of the metal particle in concern. However, the absorption coefficient crucially depends on the radius of the metal particle as described in the following model given in Eq. (2), through the volume of the gold particle V_{NP} [44, 45]:

$$\alpha(\lambda) = 3\varepsilon_m(\lambda) V_{NP} \frac{\varepsilon(\lambda) - \varepsilon_m(\lambda)}{\varepsilon(\lambda) + \chi\varepsilon_m(\lambda)}. \tag{2}$$

Eq. (2) describes the polarization of the electron cloud distortion of the metal nanoparticle, which emerges due to the interaction of the surface plasmons with the electric field [44, 45].

Here λ is the wavelength of light, ε_m is the dielectric constant of the surrounding non-absorbing medium (Im $[\varepsilon_m] = 0$), χ is the geometric factor ($= 2$ for sphere) and $\varepsilon(\lambda)$ is a complex dielectric function depending on the wavelength of the light waves interacting with the metal particle. This function consists of real and imaginary parts and is expressed by Eq. (3) according to the Drude-Lorentz model, which is expressed in terms of frequency as a dependent variable [46]:

$$\varepsilon(\omega) = \mathrm{Re}[\varepsilon(\omega)] + i\mathrm{Im}[\varepsilon(\omega)] = 1 - \frac{\omega_p}{(\omega^2 + i\omega\gamma)}. \tag{3}$$

In this equation, ω_p is the bulk plasma frequency, γ is the damping rate that causes energy loss due to ohmic losses. These constants depend on the size and geometry of the metal particle [47, 48]. Using Eq. (2), quasistatic extinction cross-section for a spherical gold nanoparticle is obtained as given in Eq. (4) [49, 50].

$$\sigma_{EXT}(\lambda) = \frac{18\pi[\varepsilon_m(\lambda)]^{3/2}}{\lambda} V_{NP} \frac{\mathrm{Im}[\varepsilon(\lambda)]}{[\mathrm{Re}[\varepsilon(\lambda)] + 2\varepsilon_m(\lambda)]^2 + [\mathrm{Im}[\varepsilon(\lambda)]]^2} \tag{4}$$

Stimulation of the localized surface plasmon occurs when the extinction cross-sectional area is maximum; that is, the denominator of the right side of the equation is minimum [44, 45]. If the imaginary part of the dielectric function of the metal (Im $[\varepsilon(\lambda)]$) is small compared to the other term in the denominator; this minimum value can be obtained approximately at the wavelength for which Eq. (5) is valid [51]:

$$\mathrm{Re}[\varepsilon(\lambda)] \approx -2\varepsilon_m(\lambda) \tag{5}$$

Eq. (5) is also known as the Fröhlich Equation which describes the resonance wavelength condition of the localized surface plasmon [51].

The above theoretical procedure is employed to optimize the efficiency of the photonic device through the fine-tuning of the diameter of the gold nanoparticle. According to our results, the local electric field near the gold nanoparticle is observed to be significantly enhanced when the gold nanoparticle with a diameter of 19 nm is used.

When a dipole is placed inside a photonic resonator, the Purcell factor is determined by the following well-known formula at the resonant frequency between the dipole and the cavity mode field provided that the dipole is oriented with respect to the mode field direction, as given in Eq. (6) [52]:

$$F_p = \frac{3Q(\lambda_c/n)^3}{4\pi^2 V}, \tag{6}$$

here, n is the refractive index of the cavity, V is the optical mode volume and λ_c is the cavity resonance frequency, which is equal to 561.5 nm. It is determined by taking the Fourier transform of the signal. Q-factor is calculated using the envelope of the decaying signal of the field.

Due to presence of the plasmonic nanoparticle, the mode volume of the hybrid mode is calculated, based on Eq. (7), in which the Drude model is used for the complex dielectric function [47]:

$$V = \frac{\int \left[\tilde{\mathbf{E}} \cdot \frac{\partial(\omega\varepsilon)}{\partial\omega}\tilde{\mathbf{E}} - \tilde{\mathbf{H}} \cdot \frac{\partial(\omega\mu)}{\partial\omega}\tilde{\mathbf{H}}\right] d^3\mathbf{r}}{2\varepsilon_0 n^2 [\tilde{\mathbf{E}}(\mathbf{r}_0) \cdot \mathbf{u}]^2} \tag{7}$$

Our results show that the gold nanoparticle localizes the cavity field in a very small volume through the plasmonic effect, which, as a result, dramatically decreases the mode volume of the photonic device to a value of 0.8 $(\lambda/n)^3$ with a negligible imaginary part. Also, the quality factor of the hybrid photonic-plasmonic structure is also calculated to be $1.32 \times 10^5 \pm 11.81$, which is observed not to be reduced significantly. Thus, the numerical analyses demonstrate that an enhancement of the Purcell factor of 1.3×10^4 is achieved in the designed photonic structure which is at least four times higher than that of the previously reported values for an encapsulated photonic crystal [14, 35, 38].

Perspective views of the hybrid resonator, which consists of a photonic crystal resonator and a gold nanoparticle at distant and close-ranges are given in Figure 7a and 7b, respectively. The inset figure given in Figure 7a shows the dimensions of the gold nanoparticle, used in the simulations. The plasmonic nanoparticle, with the optimized diameter of 19 nm, is placed on the surface of the PMMA layer at the central region of the photonic crystal waveguide, as shown in Figure 7a and 7b. The localized surface plasmons of the gold nanoparticle on the PMMA layer interact with the cavity mode field of the waveguide which naturally emerges in the z-direction.

The electric field distribution profile of the hybrid photonic-plasmonic resonator is seen in Figure 7c. The electric field distribution profile at close-range of the gold nanoparticle, placed on the surface of the photonic crystal waveguide, is also given in Figure 7d. As the cavity mode field in the resonant structure is seen in Figure 7c, the concentrated electromagnetic field around the gold nanoparticle becomes dominant in the presence of the localized surface plasmons to unveil the reproduction of the hybrid photonic-plasmonic mode, as shown in Figure 7d. Therefore, Figure 7c and 7d confirm that the plasmonic nanoparticle causes a strong confinement of the cavity mode field of the photonic crystal waveguide at nanoscale dimensions.

The PMMA layer thickness between the dipole on the surface of the photonic crystal nanocavity and the surface plasmons of the metal nanoparticle is also crucial for the enhancement of the local electromagnetic field. A smaller thickness layer of the PMMA polymer material is expected to result in a stronger field enhancement, nevertheless, the electron and energy transfer mechanisms would dominate the dipole-hybrid mode field interaction. In the modelled structure, a photonic crystal cavity with a controllable thickness of the PMMA layer between the dipole and the plasmonic nanoparticle, enables a robust and well-designed system to be used in integrated photonic platforms.

In the scientific literature, various hybrid photonic-plasmonic structures have been demonstrated to enhance spontaneous emission rate of the fluorescent quantum sources [53, 54, 55]. Some conceptually successful hybrid resonators based on 2D photonic crystal cavities with plasmonic nanoparticles have also been unveiled to enhance radiation

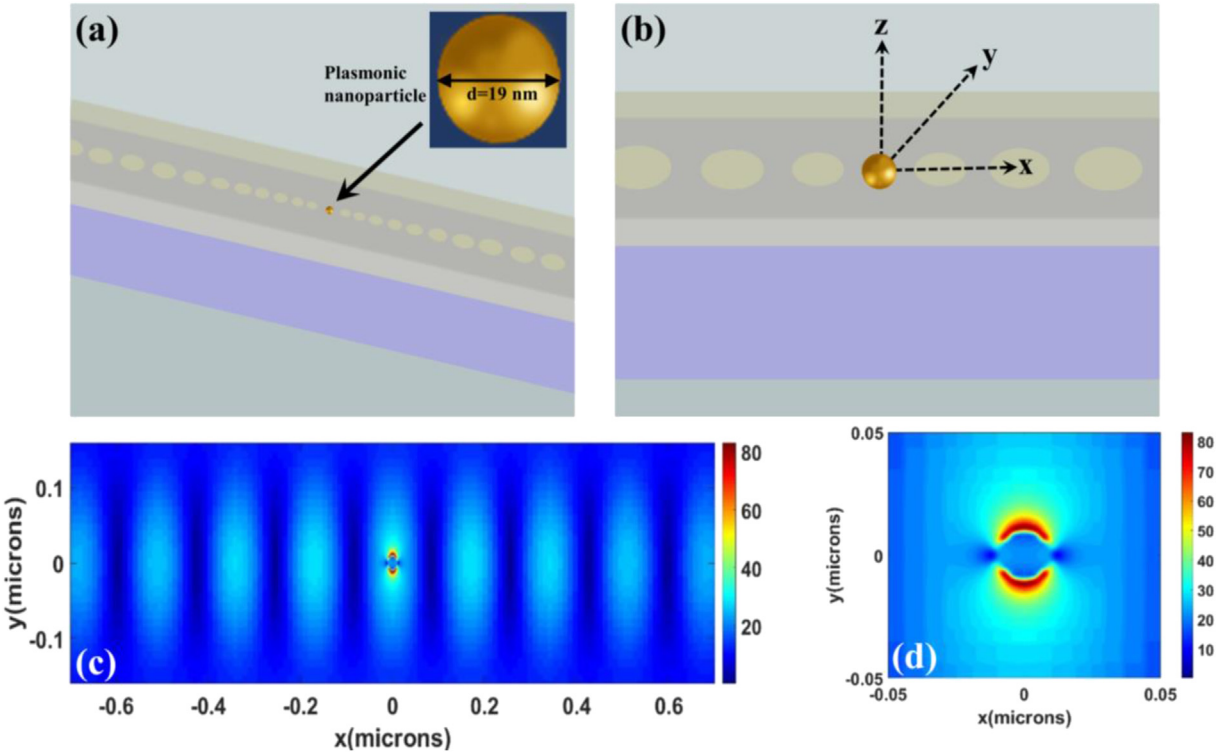

Figure 7. Perspective view of the hybrid resonator, which consists of a photonic crystal resonator and a gold nanoparticle at a) distant and b) close-range. c) The electric field distribution profile of the hybrid photonic-plasmonic cavity. d) The electric field distribution profile at close-range of the gold nanoparticle, placed on the surface of the photonic crystal structure.

efficiency [26, 27]. In these work, photonic structures are demonstrated to have low or moderate *Q*-factors. For instance, in a recent study, plasmonic rods and nanospheres, which are integrated to a 2D photonic crystal cavity, are excited to allow surface plasmons to be coupled into the cavity mode to control and considerably enhance light−matter interaction [27]. However, the *Q*-factor of the device has been shown to decrease from a value of $Q = 2500$ to $Q = 720$ in the presence of a metal nanoparticle. In another example, a 2D photonic crystal structure has been designed to originate two different cavity resonances [30]. A large bandgap Fabry-Perot cavity and a narrow bandgap photonic crystal structure are interacted with a plasmonic nanoparticle, located at the center of the structure to construct a hybrid system. According to the numerical analyses, electric field is observed to strongly localize at the surface of the plasmonic nanorods. However, the low *Q*-factor of the device ($Q = 435$) is even decreased to a value of $Q = 184$ in the hybrid resonator [30]. In our study, the reduced *Q*-factor of the device because of the encapsulation is considerably enhanced to a value of 2.05×10^5 with a design in which both sides of the nanobeam in the x-axis is chosen to be air cladding. Additionally, a hybrid system is formed by a gold nanoparticle with optimized dimensions which is integrated on the surface of the polymer layer to decrease the mode volume of the photonic device by a factor of 12. Thus, a partially encapsulated photonic crystal, with a single plasmonic nanoparticle, is proposed to have both a high *Q*-factor and a small mode volume to yield a high radiation efficiency for integrated photonic platforms.

4. Conclusions

In this paper, a partially encapsulated 1D photonic crystal nanobeam design, which offers a high *Q*-factor along with the mechanical robustness, is introduced as an alternative to air-bridged photonic crystals to enhance the radiation efficiency. A plasmonic nanoparticle is also interrogated on the surface of the nanobeam to form a hybrid photonic-plasmonic resonator. The interaction between the cavity mode and the localized surface plasmons of a gold nanoparticle integrated on the surface of the photonic crystal waveguide results in a strongly enhanced electromagnetic field through regeneration of a hybrid mode. The photonic design proposed in this paper is considered to be a key step towards the advances in fabrication of robust and efficient photonic crystal devices with a high Purcell factor for hybrid optoelectronic platforms, quantum information technologies, and laser applications.

Declarations

Author contribution statement

Belkıs Gökbulut: Conceived and designed the experiments; Performed the experiments; Analyzed and interpreted the data; Contributed reagents, materials, analysis tools or data; Wrote the paper.

Funding statement

Dr Belkıs Gökbulut was supported by TUBITAK [120F323], Bogazici University Research Fund [16761].

Data availability statement

Data will be made available on request.

Declaration of interest's statement

The author has no conflict of interest to declare.

Additional information

No additional information is available for this paper.

References

[1] S. Kumar, M. Sen, Integrable all-optical NOT gate using nonlinear photonic crystal MZI for photonic integrated circuit, J. Opt. Soc. Am. B 37 (2020) 359–369.

[2] M. Mirhosseini, A. Sipahigil, M. Kalaee, O. Painter, Superconducting qubit to optical photon transduction, Nature 588 (2020) 599–603.

[3] A. Rueda, F. Sedlmeir, M.C. Collodo, U. Vogl, B. Stiller, G. Schunk, D.V. Strekalov, C. Marquardt, J.M. Fink, O. Painter, G. Leuchs, H.G.L. Schwefel, Efficient microwave to optical photon conversion: an electro-optical realization, Optica 3 (2016) 597–604.

[4] F. Zhang, J. Ren, L. Shan, X. Duan, Y. Li, T. Zhang, Q. Gong, Y. Gu, Chiral cavity quantum electrodynamics with coupled nanophotonic structures, Phys. Rev. A 100 (2019), 053841.

[5] J.P. Vasco, S. Hughes, Anderson localization in disordered *LN* photonic crystal slab cavities, ACS Photon. 5 (2018) 1262–1272.

[6] S. Mandal, X. Serey, D. Erickson, Nanomanipulation using silicon photonic crystal resonators, Nano Lett. 10 (2009) 99–104.

[7] S. John, O. Toader, K. Busch, Photonic band gap materials: a semiconductor for light, Encycl. Phys. Sci.Technol. 12 (2001).

[8] T.K. Fryett, K.L. Seyler, J. Zheng, C.-H. Liu, X. Xu, A. Majumdar, Silicon photonic crystal cavity enhanced second-harmonic generation from monolayer WSe_2, 2D Mater. 4 (2016), 015031.

[9] F. Liu, A.J. Brash, J. O'Hara, L.M.P.P. Martins, C.L. Phillips, R.J. Coles, B. Royall, E. Clarke, C. Bentham, N. Prtljaga, I.E. Itskevich, L.R. Wilson, M.S. Skolnick, A.M. Fox, High Purcell factor generation of indistinguishable on-chip single photons, Nat. Nanotechnol. 13 (2018) 835–840.

[10] T. Li, D. Gao, D. Zhang, E. Cassan, High- *Q* and high-sensitivity one-dimensional photonic crystal slot nanobeam cavity sensors, IEEE Photon. Technol. Lett. 28 (2015) 689–692.

[11] J. Olthaus, P.P.J. Schrinner, D.E. Reiter, C. Schuck, Optimal photonic crystal cavities for coupling nanoemitters to photonic integrated circuits, Adv. Quantum Technol. 3 (2019), 1900084.

[12] W. Zhou, Encapsulated Photonic Crystals for High Efficiency Nanolasers, Nanoengineering: Fabrication, Properties, Optics, and Devices II, SPIE, 2005, p. 59310A.

[13] A. Bazin, R. Raj, F. Raineri, Design of silica encapsulated high-*Q* photonic crystal nanobeam cavity, J. Lightwave Technol. 32 (2013) 952–958.

[14] Y. Chen, A. Ryou, M.R. Friedfeld, T. Fryett, J. Whitehead, B.M. Cossairt, A. Majumdar, Deterministic positioning of colloidal quantum dots on silicon nitride nanobeam cavities, Nano Lett. 18 (2018) 6404–6410.

[15] R. Miura, S. Imamura, R. Ohta, A. Ishii, X. Liu, T. Shimada, S. Iwamoto, Y. Arakawa, Y.K. Kato, Ultralow mode-volume photonic crystal nanobeam cavities for high-efficiency coupling to individual carbon nanotube emitters, Nat. Commun. 5 (2014) 5580.

[16] W.S. Fegadolli, J.E.B. Oliveira, V.R. Almeida, A. Scherer, Compact and low power consumption tunable photonic crystal nanobeam cavity, Opt Express 21 (2013) 3861–3871.

[17] J.D. Ryckman, S.M. Weiss, Low mode volume slotted photonic crystal single nanobeam cavity, Appl. Phys. Lett. 101 (2012), 071104.

[18] M.W. McCutcheon, D.E. Chang, Y. Zhang, M.D. Lukin, M. Loncar, Broadband frequency conversion and shaping of single photons emitted from a nonlinear cavity, Opt Express 17 (2009) 22689–22703.

[19] K. Rivoire, S. Buckley, J. Vučković, Multiply resonant photonic crystal nanocavities for nonlinear frequency conversion, Opt Express 19 (2011) 22198–22207.

[20] H. Li, M. Li, Optomechanical photon shuttling between photonic cavities, Nat. Nanotechnol. 9 (2014) 913–919.

[21] J. Hendrickson, R. Soref, J. Sweet, W. Buchwald, Ultrasensitive silicon photonic-crystal nanobeam electro-optical modulator: design and simulation, Opt Express 22 (2014) 3271–3283.

[22] P. Lee, T. Lu, L. Chiu, Dielectric-band photonic crystal nanobeam lasers, J. Lightwave Technol. 31 (2013) 36–42.

[23] Q. Quan, Single particle detection in CMOS compatible photonic crystal nanobeam cavities, Opt Express 21 (2013) 32225–32233.

[24] F. Liang, N. Clarke, P. Patel, M. Loncar, Q. Quan, Scalable photonic crystal chips for high sensitivity protein detection, Opt Express 21 (2013) 32306–32312.

[25] Q. Quan, P.B. Deotare, L. Marko, Photonic crystal nanobeam cavity strongly coupled to the feeding waveguide, Appl. Phys. Lett. 96 (2010), 203102.

[26] J.-N. Liu, Q. Huang, K.-K. Liu, S. Singamaneni, B.T. Cunningham, Nanoantenna-microcavity hybrids with highly cooperative plasmonic-photonic coupling, Nano Lett. 17 (2010) 7569–7577.

[27] J. Do, K.N. Sediq, K. Deasy, D.M. Coles, J. Rodriguez-Fernandez, J. Feldmann, D.G. Lidzey, Photonic crystal nanocavities containing plasmonic nanoparticles assembled using a laser-printing technique, Adv. Opt. Mater. 1 (2013) 946–951.

[28] M.T. Hill, Y.-S. Oei, B. Smalbrugge, Y. Zhu, T. de Vries, P.J. van Veldhoven, F.W.M. van Otten, T.J. Eijkemans, J.P. Turkiewicz, H. de Waardt, E.J. Geluk, S.-H. Kwon, Y.-H. Lee, R. Nötzel, M.K. Smit, Lasing in metallic-coated nanocavities, Nat. Photonics 1 (2007) 589–594.

[29] D. Conteduca, C. Reardon, M.G. Scullion, F. Dell'Olio, M.N. Armenise, Ultra-high Q/V hybrid cavity for strong light-matter interaction, APL Photonics 2 (2017), 086101.

[30] M. Barth, S. Schietinger, S. Fischer, J. Becker, N. Nüsse, T. Aichele, B. Löchel, C. Sönnichsen, O. Benson, Nanoassembled plasmonic-photonic hybrid cavity for tailored light-matter coupling, Nano Lett. 10 (2010) 891–895.

[31] Z. Yang, M. Pelton, I. Fedin, D.V. Talapin, E. Waks, A room temperature continuous-wave nanolaser using colloidal quantum wells, Nat. Commun. 8 (2017) 143.

[32] W. Zhu, R. Esteban, A.G. Borisov, J.J. Baumberg, P. Nordlander, H.J. Lezec, J. Aizpurua, K.B. Crozier, Quantum mechanical effects in plasmonic structures with subnanometer gaps, Nat. Commun. 7 (2016), 11495.

[33] J.F. Bauters, M.J.R. Heck, D. John, D. Dai, M.-C. Tien, J.S. Barton, A. Leinse, R.G. Heideman, D.J. Blumenthal, J.E. Bowers, Ultra-low-loss high-aspect-ratio Si_3N_4 waveguides, Opt Express 19 (2011) 3163–3174.

[34] M. Grande, G. Calo, V. Petruzzelli, A. D'Orazio, High-*Q* photonic crystal nanobeam cavity based on a silicon nitride membrane incorporating fabrication imperfections and a low-index material layer, Prog. Electromagn. Res. 37 (2012) 191–204.

[35] D. Panettieri, L. O'Faolain, M. Grande, Control of *Q*-Factor in Nanobeam Cavities on Substrate, 18th International Conference on Transparent Optical Networks (ICTON), IEEE, 2016, pp. 2161–2164.

[36] T.K. Fryett, Y. Chen, Z.M. Peycke, X. Xu, A. Majumdar, Encapsulated silicon nitride nanobeam cavity for hybrid nanophotonics, ACS Photonics 5 (2018) 2176–2181.

[37] P. Lalanne, C. Sauvan, J.P. Hugonin, Photon confinement in photonic crystal nanocavities, Laser Photon. Rev. 2 (2008) 514–526.

[38] T.K. Fryett, Y. Chen, J. Whitehead, Z.M. Peycke, X. Xu, A. Majumdar, Encapsulated Silicon Nitride Nanobeam Cavity for Nanophotonics Using Layered Materials, in: CLEO: Science and Innovations, 2018. JW2A.16.

[39] R. Gansch, S. Kalchmair, H. Detz, A.M. Andrews, P. Klang, W. Schrenk, G. Strasser, Higher order modes in photonic crystal slabs, Opt Express 19 (2011) 15990–15995.

[40] T. Zhou, M. Tang, G. Xiang, B. Xiang, S. Hark, M. Martin, T. Baron, S. Pan, J.-S. Park, Z. Liu, S. Chen, Z. Zhang, H. Liu, Continuous-wave quantum dot photonic crystal lasers grown on on-axis Si (001), Nat. Commun. 11 (2020) 977.

[41] Y. Gong, B. Ellis, G. Shambat, T. Sarmiento, J.S. Harris, J. Vučković, Nanobeam photonic crystal cavity quantum dot laser, Opt Express 18 (2010) 8781–8789.

[42] Y.-F. Xiao, Y.-C. Liu, B.-B. Li, Y.-L. Chen, Y. Li, Q. Gong, Strongly enhanced light-matter interaction in a hybrid photonic-plasmonic resonator, Phys. Rev. A 85 (2012), 031805.

[43] A. Samanta, Y. Zhou, S. Zou, H. Yan, Y. Liu, Fluorescence quenching of quantum dots by gold nanoparticles: a potential long range spectroscopic ruler, Nano Lett. 14 (2014) 5052–5057.

[44] U. Kreibig, M. Vollmer, Optical Properties of Metal Clusters, Springer Science & Business Media, Berlin, 2013.

[45] K.M. Mayer, J.H. Hafner, Localized surface plasmon resonance sensors, Chem. Rev. 111 (2011) 3828–3857.

[46] R.L. Olmon, B. Slovick, T.W. Johnson, D. Shelton, S.-H. Oh, G.D. Boreman, M.B. Raschke, Optical dielectric function of gold, Phys. Rev. B 86 (2012), 235147.

[47] C. Sauvan, J.P. Hugonin, I.S. Maksymov, P. Lalanne, Theory of the spontaneous optical emission of nanosize photonic and plasmon resonators, Phys. Rev. Lett. 110 (2013), 237401.

[48] A. Derkachova, K. Kolwas, I. Demchenko, Dielectric function for gold in plasmonics applications: size dependence of plasmon resonance frequencies and damping rates for nanospheres, Plasmonics 11 (2016) 941–951.

[49] S.A. Maier, Plasmonics: Fundamentals and Applications, Springer Science & Business Media, Berlin, 2007.

[50] C.F. Bohren, D.R. Huffman, Absorption and Scattering of Light by Small Particles, John Wiley & Sons, New Jersey, USA, 2008.

[51] V. Amendola, R. Pilot, M. Frasconi, O.M. Maragò, M.A. Iatì, Surface plasmon resonance in gold nanoparticles: a review, J. Phys. Condens. Matter 29 (2017), 203002.

[52] E.M. Purcell, Spontaneous emission probabilities at radio frequencies, Phys. Rev. 69 (1946) 681.

[53] B. Gökbulut, A. Inanc, G. Topcu, S.S. Unluturk, S. Ozcelik, M.M. Demir, M.N. Inci, Enhanced spontaneous emission rate in a low-Q hybrid photonic-plasmonic nanoresonator, J. Phys. Chem. C 123 (2019) 19862–19870.

[54] B. Gökbulut, A. Inanc, G. Topcu, S. Ozcelik, M.M. Demir, M.N. Inci, Hybrid photonic-plasmonic mode coupling induced enhancement of the spontaneous emission rate of CdS/CdSe quantum emitters, Phys. E Low Dimens. Syst. Nanostruct. 136 (2022), 115017.

[55] B. Gökbulut, A. Inanc, G. Topcu, S. Ozcelik, M.M. Demir, M.N. Inci, Enhanced light–matter interaction in a hybrid photonic–plasmonic cavity, Appl. Phys. A 127 (2021) 907.